# ARTICLE  OPEN

# Wafer-scale two-dimensional ferromagnetic Fe$_3$GeTe$_2$ thin films grown by molecular beam epitaxy

Shanshan Liu[1,2], Xiang Yuan[1,2], Yichao Zou[3], Yu Sheng[4], Ce Huang[1,2], Enze Zhang[1,2], Jiwei Ling[1,2], Yanwen Liu[1,2], Weiyi Wang[1,2], Cheng Zhang[1,2], Jin Zou[3,5], Kaiyou Wang[4] and Faxian Xiu[1,2,6]

Recently, layered two-dimensional ferromagnetic materials (2D FMs) have attracted a great deal of interest for developing low-dimensional magnetic and spintronic devices. Mechanically exfoliated 2D FMs were discovered to possess ferromagnetism down to monolayer. It is therefore of great importance to investigate the distinct magnetic properties at low dimensionality. Here, we report the wafer-scale growth of 2D ferromagnetic thin films of Fe$_3$GeTe$_2$ via molecular beam epitaxy, and their exotic magnetic properties can be manipulated via the Fe composition and the interface coupling with antiferromagnetic MnTe. A 2D layer-by-layer growth mode has been achieved by in situ reflection high-energy electron diffraction oscillations, yielding a well-defined interlayer distance of 0.82 nm along {002} surface. The magnetic easy axis is oriented along $c$-axis with a Curie temperature of 216.4 K. Remarkably, the Curie temperature can be enhanced when raising the Fe composition. Upon coupling with MnTe, the coercive field dramatically increases 50% from 0.65 to 0.94 Tesla. The large-scale layer-by-layer growth and controllable magnetic properties make Fe$_3$GeTe$_2$ a promising candidate for spintronic applications. It also opens up unprecedented opportunities to explore rich physics when coupled with other 2D superconductors and topological matters.

## INTRODUCTION

With the discovery of graphene and its astonishing physical properties,[1] a new class of two-dimensional (2D) materials, ascribed to the dimensionality effect and modulation in their band structures, has become the focus of intense research which ranges from 2D semiconductors, like black phosphorous,[2] MoS$_2$,[3] and WSe$_2$,[4–6] to 2D superconductors, for example, NbSe$_2$,[7, 8] and FeSe.[9–11] The 2D ferromagnetic materials (2D FMs),[12] were predicted to have promising spintronic applications[13–16] with stable storage, faster response and low-power dissipation.[12, 17] To this end, two approaches are currently adopted involving the introduction of defects or adatoms into parent materials or the proximity effect with ferromagnetic materials,[18] for instance, the ferromagnetism in NbSe$_2$ through hydrogen absorbed on the surface,[19] and the search for the intrinsic magnetic materials. However, the resulting ferromagnetic materials by the former method significantly suffer from the undesired stability and limited controllability. To date, the predicted possible categories of 2D intrinsic FMs are mainly made up of Fe$_3$GeTe$_2$[20, 21] and CrXTe$_3$ (X = Si, Sn, Ge)[22–24] with the calculated Curie temperature of 220 K (bulk),[25, 26] 90 K (monolayer),[24] 170 K (monolayer),[22] and 130 K (monolayer).[24]

Experimentally, some progress has been made. By reducing the sample thickness,[18] V$_5$S$_8$ changes from antiferromagnetic to ferromagnetic states. Through previous ferromagnetic resonance (FMR) study,[17] the exfoliated CrGeTe$_3$ exhibits a Curie temperature around 61 K with an uniaxial magnetic property which can be tuned by external magnetic field.[27] Even down to bilayer and monolayer, CrGeTe$_3$, and CrI$_3$ are still in the ferromagnetic state with a Curie temperature of 30 [27] and 45 K,[28] respectively, which is much lower than their bulk counterparts. Recently, the reported field-effect transistors based on ferromagnetic semiconductor C$_3$N quantum dots (QDs)[29] show an on–off ratio around $10^{10}$ with the tunable bandgap ranging from visible to infrared light for different-size QDs. However, the experimental progress in producing large-scale 2D FM thin films remains an obstacle. So far, the ferromagnetic single crystals such as Fe$_3$GeTe$_2$ and CrGeTe$_3$ were mainly developed by chemical vapor transport (CVT).[17, 25] Due to the van der Waals interaction between layers, these materials can be easily exfoliated by the Scotch-tape method, but yet, the resultant nano-devices are largely restricted by the sample size.[30] Thus, the successful growth of large-scale 2D FM thin films becomes a thrust theme as it not only boosts the rapid exploration of physics but also renders the possibility to investigate various heterojunctions.[12] For instance, by coupling with topological insulators, it is possible to probe quantized anomalous Hall effect and magnetic monopoles.[31, 32] With superconductors, Andreev reflection effect[7, 33] and the super-exchange interaction[34, 35] can be investigated through the proximity effect. Besides the exotic physics, the molecular beam epitaxy (MBE) is well established in growing highly uniform and crystalline quality films. For the 2D materials, the thickness can be well controlled through the in situ reflection high-energy electron diffraction (RHEED) oscillations. These outstanding superiorities make MBE a desirable technique for producing wafer-scale-size films with well-defined thickness controllability.

[1]State Key Laboratory of Surface Physics and Department of Physics, Fudan University, Shanghai 200433, China; [2]Institute for Nanoelectronic Devices and Quantum Computing, Fudan University, Shanghai 200433, China; [3]Materials Engineering, The University of Queensland, Brisbane, QLD 4072, Australia; [4]SKLSM, Institute of Semiconductors, Chinese Academy of Sciences, Beijing 100083, China; [5]Centre for Microscopy and Microanalysis, The University of Queensland, Brisbane, QLD 4072, Australia and [6]Collaborative Innovation Center of Advanced Microstructures, Nanjing 210093, China
Correspondence: Kaiyou Wang (kywang@semi.ac.cn) or Faxian Xiu (Faxian@fudan.edu.cn)

npj

Wafer-scale two-dimensional ferromagnetic Fe$_3$GeTe$_2$
Shanshan Liu et al.

2

Compared with other ferromagnetic materials such as CrSiTe$_3$ and CrGeTe$_3$, Fe$_3$GeTe$_2$ possesses outstanding properties. First, its superior stability is confirmed by the non-imaginary frequencies in phonon spectrum calculations.[20] Indeed, the oxidation process of Fe$_3$GeTe$_2$ in our experiments is slower in comparison with CrGeTe$_3$. Second, it is predicted to be an itinerant ferromagnet with a relatively high-Curie temperature around 220 K.[26] Essentially, this becomes a very important figure of merit for spin-based technology architecture. Third, the anisotropy energy of Fe$_3$GeTe$_2$ around $10^7$ erg/cm$^3$ determined by magnetic force microscope[36] is much larger than that of CrGeTe$_3$ with $10^5$ erg/cm$^3$ measured with FMR,[17] which is critical for magnetic tunnel junctions and magnetic random access memory devices. All of them require a large difference between anisotropy energy and thermal activation energy $k_BT$ for stable storage.[20] In addition, the perpendicular magnetic anisotropy provides lower switching current in comparison with the in-plane one.[37, 38]

Here, we investigate 2D FM Fe$_3$GeTe$_2$ thin films grown on sapphire and GaAs by MBE. Periodic in situ RHEED oscillations clearly demonstrate the 2D growth mode through which the thickness of Fe$_3$GeTe$_2$ films can be precisely determined. Our low-temperature transport experiments unveil the out-of-plane easy axis along $c$ direction with the Curie temperature of 216.4 K. And importantly, the Curie temperature is found to vary systematically with the Fe composition. By constructing a superlattice-like structure of (Fe$_3$GeTe$_2$/MnTe)$_3$, where the subscript 3 means three periods of Fe$_3$GeTe$_2$/MnTe, the coercive field of Fe$_3$GeTe$_2$ increases 50%, exhibiting a tunable magnetic states.

## RESULTS AND DISCUSSION

Two-inch high-crystalline-quality Fe$_3$GeTe$_2$ films were grown in a high-vacuum MBE system. Figure 1a shows the crystal structure geometry, which belongs to a space group P6$_3$/mmc. Each layer consists of five sublayers with sandwich-like stacking order. The lattice constants are $a = b = 3.9536(7)$ Å and $c = 16.396(2)$ Å. The top view displays a hexagonal distribution of atoms, as shown in the top panel of Fig. 1a. The inset of Fig. 1b exhibits a typical RHEED pattern obtained during the growth, where the streaky stripes suggest the atomically smooth surface and indicate the high-crystalline quality. These properties are further demonstrated by X-ray diffraction (XRD) and high-resolution transmission electron microscope (HRTEM). Figure 1b shows in situ RHEED oscillations and the equal periodicity provides a strong evidence of 2D growth mode. We note that it typically takes 111 s to complete one layer growth, suggesting that the thickness of Fe$_3$GeTe$_2$ films can be well controlled. Due to the low XRD intensity of 8 nm film, a thicker sample on sapphire under the same growth condition is used for the XRD measurements, as shown in Fig. 1c. According to PDF Card #75-5620 and the published XRD data of single crystals,[26] peaks marked in red can be ascribed to a series of {002} planes—(002), (004), (008), (0010), and (0014), suggesting that Fe$_3$GeTe$_2$ is single crystalline and the growth is along $c$ axis. Other peaks marked in blue are originated from the sapphire substrate. HRTEM experiments were further carried out to determine the layered structure of the Fe$_3$GeTe$_2$ film on (111) GaAs (Fig. 1d). The upper inset of Fig. 1d is the HRTEM taken from the Fe$_3$GeTe$_2$ region in which a van der Waals gap of 0.82 nm can be observed, corresponding to the (0002) displacing
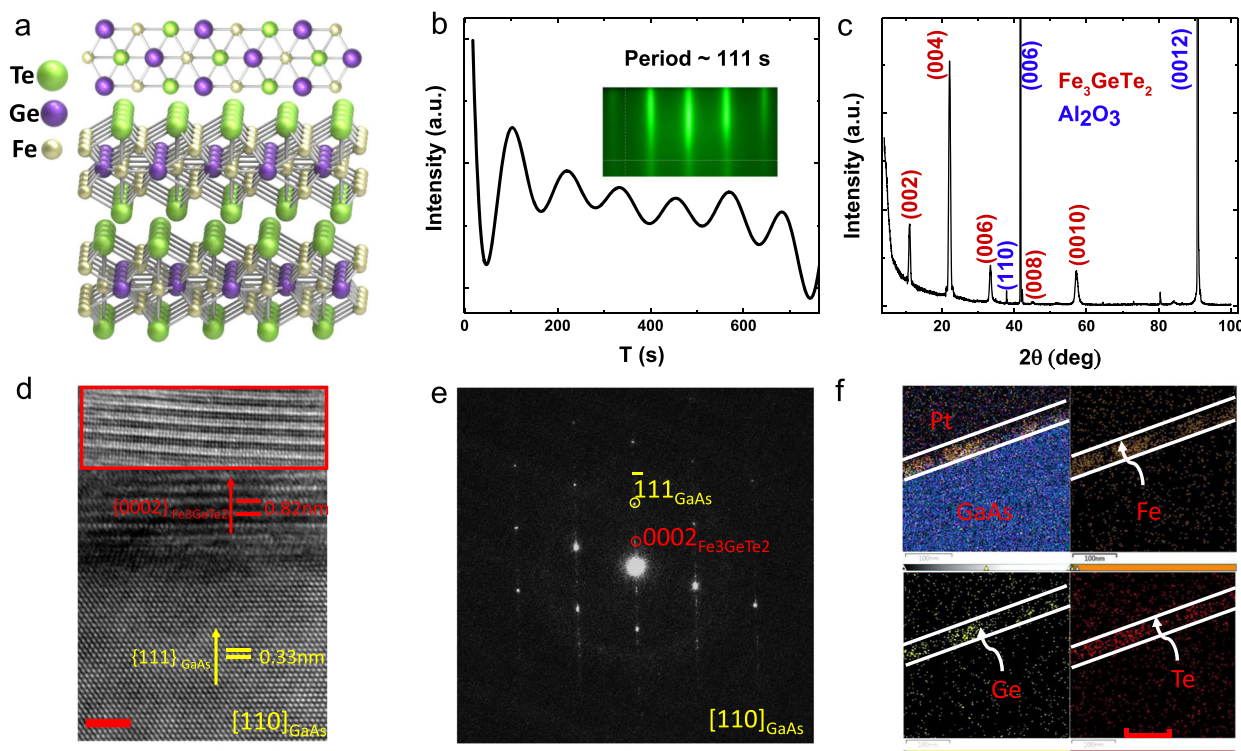


**Fig. 1** Fe$_3$GeTe$_2$ thin film growth and characterizations. **a** Structure geometry of Fe$_3$GeTe$_2$, terminated with Te layer. The top panel is a top view, where the hexagonal distribution can be observed clearly. **b** RHEED oscillations. By the periodic oscillations, the 2D epitaxial mode can be verified and the growth period per layer is 111 s. The inset is the RHEED picture with streaky stripes, demonstrating the smooth surface condition. **c** XRD data, compared with the PDF Card #75-5620 and the reported single crystals, the orientation can be determined to be along [002] directions, marked in *red*. **d** Cross-section HRTEM images taken from the interface area of the Fe$_3$GeTe$_2$ thin film grown on (111) GaAs with the scale bar of 2 nm. The upper inset marked by a *red* rectangle is taken from the Fe$_3$GeTe$_2$ region, indicating its layer distance is 0.82 nm, corresponding to {0002}$_{Fe3GeTe2}$. **e** Corresponding SAED. **f** EDS mapping results, displaying uniform distribution of Fe, Ge, and Te atoms in the film, marked as the region between the marked *white* lines. The scale bar is 100 nm. Note that the Pt layer is deposited during the TEM sample preparation by focused ion beam (FIB)

Wafer-scale two-dimensional ferromagnetic Fe₃GeTe₂
Shanshan Liu et al.

npj

3

of Fe₃GeTe₂.[20] Figure 1d shows the HRTEM image taken from the interface region between Fe₃GeTe₂ film and GaAs substrate, taken from GaAs {110} axis. The corresponding selected area electron diffraction (SAED) taken from the interface region is presented in Fig. 1e, from which the crystallographic relationship between the Fe₃GeTe₂ film and GaAs can be determined as {0001}$_{Fe3GeTe2}$// {111}$_{GaAs}$. Energy-dispersive X-ray spectroscopy (EDS) maps taken from the film region confirms the uniform elemental distribution of Fe, Ge, and Te in the film, as shown in Fig. 1f. With all the above characterizations, the Fe₃GeTe₂ thin films are found to grow uniformly on the substrate, and have a high-crystalline quality.

To explore low-temperature electrical properties, two-inch Fe₃GeTe₂ films were cut into small pieces and fabricated into a Hall-bar structure (Fig. 2a inset). Figure 2a shows the temperature-dependent resistance (R-T) data of 8 nm Fe₃GeTe₂ on Al₂O₃. Consistent with the theoretical predictions,[21] with decreasing temperature the resistance decreases, showing a metallic behavior. However, upon reaching ~ 40 K, the R-T curve exhibits an upward increase. The inset shows a fit to the Mott's variable range hopping (VRH) model yielding $\ln(R_{xx}) \sim T^{-1/3}$, where 1/3 is characteristic for 2D materials and it would be 1/4 for 3D materials, which means that at low temperatures the localized carriers hop to the lowest activation energy states other than the nearest-neighboring states. A similar transport behavior was also observed in other material systems.[39–41]

To investigate the ferromagnetic properties, a magnetic field up to ±9 T is scanned back and forth. Generally, the Hall effect of ferromagnetic materials can be described by[42] $R_{xy} = R_H B + R_{AH} M$, where $R_H$ stands for the normal Hall contribution, and $R_{AH}$ comes from the magnetization contribution. Subtracting the normal Hall slopes from the raw data yields the anomalous Hall signals that are also dependent on the angle between magnetic field (B) and

the normal vector of the sample surface (Fig. 2b and inset). It is evident that the easy axis of Fe₃GeTe₂ is along c-axis (out-of-plane) as the coercive field ($H_c$) increases simultaneously with the angle. When raising the temperature, $H_c$ decreases and will reach zero at the Curie temperature, as shown in Fig. 2c and e, respectively. Based on that, the Curie temperature can be roughly estimated. More precise determination of Curie temperature can be achieved by the Arrott-plot, as described later. At 2 K, the hole carrier density and mobility were extracted to be $1.2 \times 10^{19}$ cm⁻³ and 54.9 cm² V⁻¹ s⁻¹, respectively, as displayed in Fig. 2d.

To estimate the Curie temperature and compare it with that of the bulk crystal counterpart, the method of the Arrott-plot has been adopted.[41] First $(R_{xy}/R_{xx}^2)^2$ is plotted against $B/(R_{xy}/R_{xx}^2)$. It is well known that the intercept is positive for ferromagnetic and negative for paramagnetic state.[43] Then, the Curie temperature $T_c$ can be extracted when the intercept on the $(R_{xy}/R_{xx}^2)^2$ axis goes to zero. Figure 3a shows $(R_{xy}/R_{xx}^2)^2 \sim B/(R_{xy}/R_{xx}^2)$ curves of 70, 100, 125, 150, 180, and 200 K, and the intercept, determined from these linear fittings (Fig. 3b), decreases when the temperature increases. Using a liner fit, the Curie temperature is determined to be 216.4 ± 0.4 K.

Superconducting quantum interference device (SQUID) was used to measure the magnetic properties. Since the easy axis of Fe₃GeTe₂ films is out-of-plane, the magnetic field is set to be perpendicular to the sample surface (perpendicular geometry). Figure 3c displays the Zero-field-cooling (ZFC) and field-cooling (FC) curves under 100 Oe for 8-nm Fe₃GeTe₂ grown on sapphire substrate. With decreasing the temperature, the magnetization under field-cooling process increases, showing an opposite trend to the ZFC curve. The Curie temperature can be roughly determined to be ~ 212.8 K, comparable to 216.4 K determined by transport Hall results. Magnetization hysteresis was achieved by
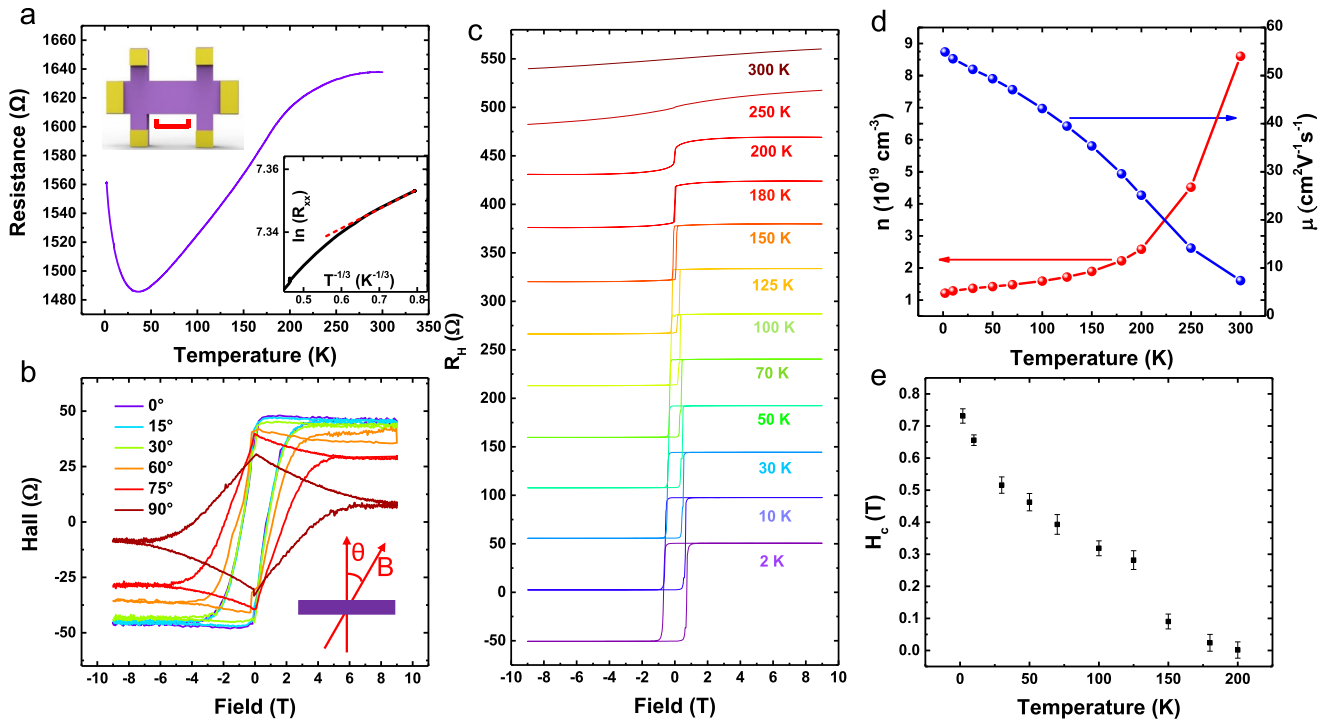


**Fig. 2** Transport properties of 8 nm Fe₃GeTe₂ thin film. **a** R-T curve, showing a metallic characteristic. The bottom inset is a fit to the variable range hopping model, $\ln(R_{xx}) \sim T^{-1/3}$. The scale bar of the top inset Hall-bar structure is 1 mm. **b** Angle-dependent anomalous Hall data. The measurement geometry is displayed in the inset. With magnetic field changing from perpendicular ($\theta = 0°$) to parallel ($\theta = 90°$) to the sample surface, the coercive field increases largely, from which the easy axis can be determined to be out-of-plane. **c** Anomalous Hall data at different temperatures with the offset of 50 Ω. With rising temperature, the coercive field decreases successively. The hysteresis at 200 K is very small, the coercive field at which is displayed in 2 **e**. **d** Carrier density and mobility at different temperatures. **e** Temperature-dependent coercive fields, which are calculated from anomalous Hall results (Fig. 2c). The error bars were estimated to be around 0.01 Tesla in the whole temperature range
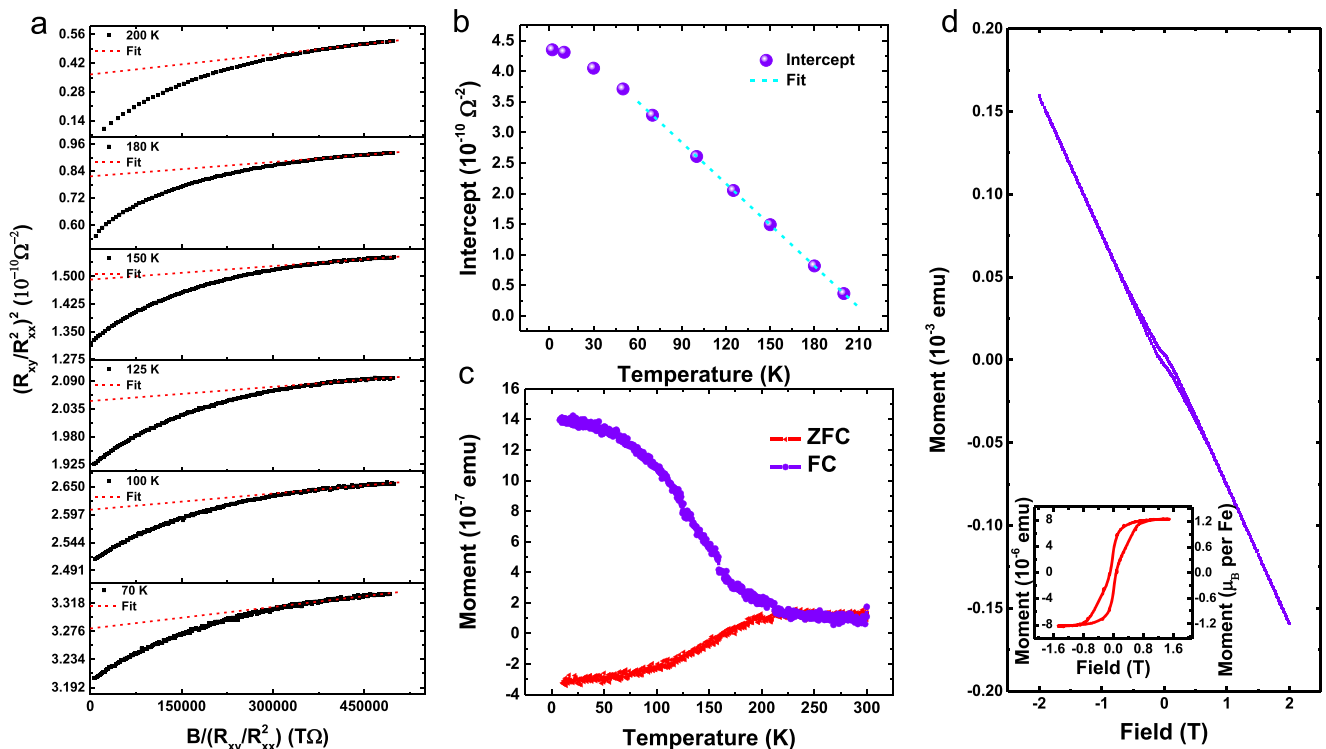
npj

Wafer-scale two-dimensional ferromagnetic Fe₃GeTe₂
Shanshan Liu et al.

4

**Fig. 3** Arrott-plots using anomalous Hall data and magnetization measured by SQUID. **a** and **b** are Arrot-plots at temperatures from 70 K to 200 K. The x-axis and y-axis are $B/(R_{xy}/R_{xx}^2)$ and $(R_{xy}/R_{xx}^2)^2$, respectively. *Dashed lines* represent the linear fits to the small-region data that near magnetization saturation. Using the intercepts in y-axis (summarized in Fig. 3b) and fitting these values in a liner relation, the Curie temperature is calculated to be 216.4 ± 0.4 K. **c** Zero-field-cooling (ZFC) and field-cooling (FC) curves under 100 Oe for 8-nm Fe₃GeTe₂ grown on sapphire substrate. For FC, with decreasing the temperature, the magnetization increases, showing an opposite trend to the ZFC curve. The Curie temperature can be roughly determined to be ~ 212.8 K, comparable to 216.4 K determined by the anomalous Hall effect measurements (Fig. 3a and b). **d** Magnetization hysteresis at 10 K. Due to the Al₂O₃ substrate, stronger diamagnetic background can be seen. After subtracting the diamagnetic background of substrate, a clear hysteresis from Fe₃GeTe₂ thin film is depicted in the inset with the saturation magnetization of 1.23 μB per Fe

scanning magnetic field back and forth in the region of ±3 Tesla at 10 K (Fig. 3d). Large diamagnetic background from Al₂O₃ can be clearly seen and subsequently subtracted to produce the net magnetization of Fe₃GeTe₂ thin films as displayed in Fig. 3d inset, with the saturation magnetization of 1.23 μB per Fe ion, smaller than that of bulk sample[21, 25] ~ 1.6 μB. The shrinking behavior in the center region suggests the mixture signals from a harder magnetic phase and a slightly softer magnetic phase similar to that occurs in MnGe[44] and [Co/Pd]IrMn,[45] which were further proved by our Kerr microscope measurements. The detailed discussions and experimental results are provided in Supplementary information I and II.

Next, we attempt to manipulate the magnetic properties of Fe₃GeTe₂ thin films by systematically altering the Fe composition (Fe₃₊δGeTe₂) and by coupling with antiferromagnetic layer MnTe. As shown in Fig. 4, with increasing the Fe composition, the Curie temperature, extracted from the Arrott-plots (Supplementary Figs. 3–7), dramatically increases. Such a trend was also observed in Fe₃₊δGeTe₂ single crystals grown by self-flux reaction method,[26] where the additional Fe doping decreases the lattice constant c while increases a.

Besides the control of the Fe composition, the heterostructure of Fe₃GeTe₂/MnTe was produced to enhance the magnetic properties via the exchange interaction from the FM/AFM interface. The detailed growth conditions and characterizations of MnTe itself are presented in Supplementary Fig. 9. The structure of MnTe is hexagonal NiAs-type[46] with the lattice constants a = b = 4.158 Å and c = 6.726 Å. The matching of the crystal structures enables the possibility of in situ growing MnTe directly on Fe₃GeTe₂. More importantly, the magnetic structure of MnTe is
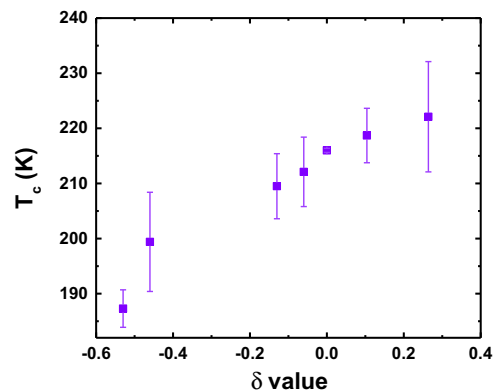


**Fig. 4** Composition-dependent Curie temperature of 8 nm Fe₃₊δGeTe₂. These Curie temperatures of different compositions were determined by Arrott-plots of transport data. With increasing the Fe composition, the Curie temperature increases. The negligible error bar for δ = 0 is 0.4 (Fe₃GeTe₂, Tc = 216.4 ± 0.4 K, shown in Fig. 2). The error bars were generated from the Arrott-plots fitting process

featured by the Mn stacking antiferromagnetically along c-axis[46] that is perfectly aligned with the easy axis of Fe₃GeTe₂. Given the fact that the Neel temperature of MnTe is 310 K, higher than the Curie temperature of Fe₃GeTe₂, we have designed several periods of Fe₃GeTe₂/MnTe and achieved such superlattices with atomically smooth interface using MBE (see the streaky RHEED patterns in Supplementary Fig. 10). From XRD, different sets of peaks from
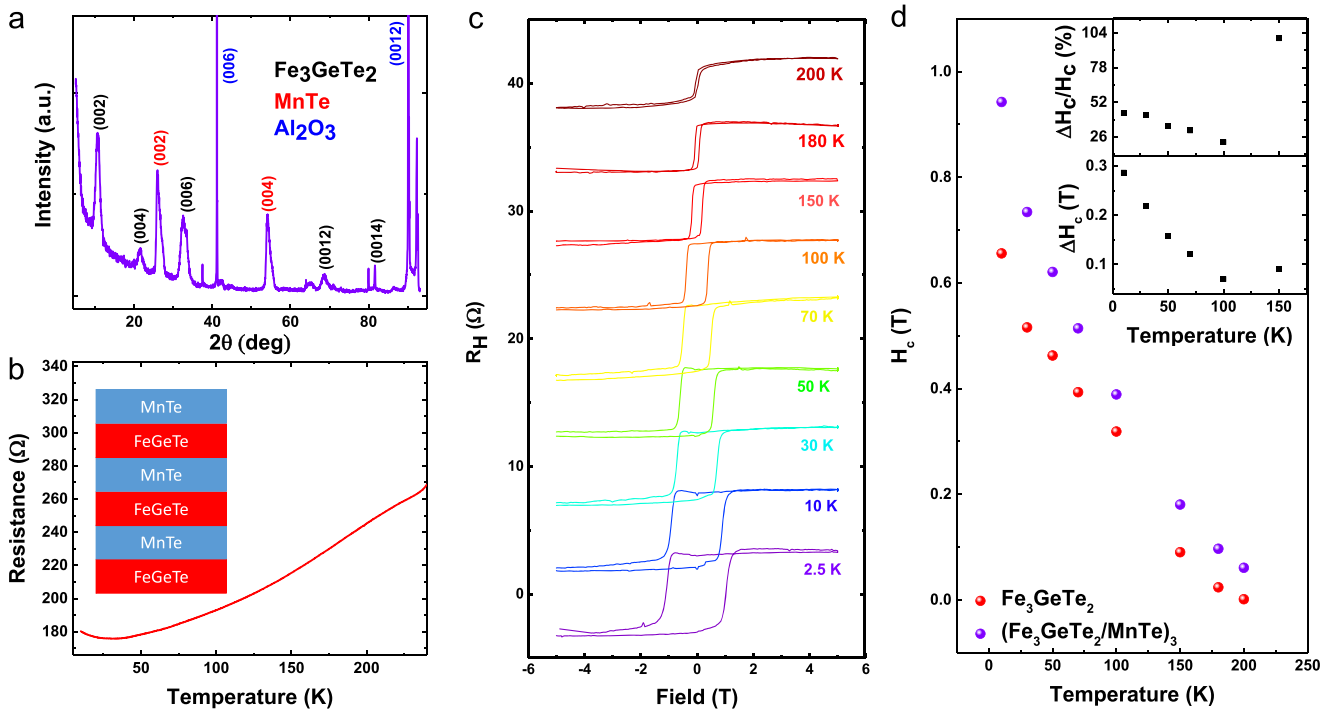
Wafer-scale two-dimensional ferromagnetic Fe₃GeTe₂
Shanshan Liu et al.

npj

5

**Fig. 5** Enhanced coercive field for a heterostructure sample (Fe₃GeTe₂/MnTe)₃. **a** XRD results. Peaks form Fe₃GeTe₂, MnTe and Al₂O₃ are marked in *black*, *red*, and *blue*, respectively. The distinguishable peaks of different class suggest the successful growth. **b** *R-T* curve of three-period Fe₃GeTe₂/MnTe heterostructure. The inset is a stacking illustration. **c** Temperature-dependent anomalous Hall results with the offset of 5 Ω. At 2.5 K, the coercive field is up to 1.1 Tesla. **d** Temperature-dependent coercive field of the pure Fe₃GeTe₂ and (Fe₃GeTe₂/MnTe)₃. With the introduction of MnTe, the coercive field increases. The top panel in the *inset* shows the increment ratio and the *bottom one* represents the absolute enhancement

Fe₃GeTe₂, MnTe and substrate Al₂O₃ can be observed (Fig. 5a). Figure 5b shows the *R-T* curve of 3-period Fe₃GeTe₂/MnTe with a metallic *R-T* behavior. Then, the angle-dependent anomalous Hall effect measurements were measured to probe the easy axis (Supplementary Fig. 11(a)) which is found to be out-of-plane. Note that hereafter the ferromagnetism measurements were always taken under the perpendicular geometry. Figure 5c displays anomalous Hall data at different temperatures. The temperature dependence of the coercive field is similar to that from the pure Fe₃GeTe₂. However, remarkably the coercive field is significantly enhanced (Fig. 5d). The inset of Fig. 5d are the absolute difference and increment ratios which are all above 50 % at different temperatures. At 10 K, the difference of the coercive field is as high as 50 % from 0.65 to 0.94 Tesla.

Conventionally, when FM and AFM are coupled, the interface interaction can induce the exchange bias and the enhanced coercive field. For the exchange bias,[47, 48] unlike the pure Fe₃GeTe₂ there will exist a shift of anomalous Hall data along *x* axis. To detect whether the exchange bias exists or not, we measured anomalous Hall data in the range of ±4 Tesla before which the sample is initially cooled down under ±5 Tesla from 350 K, well above the Neel temperature of MnTe. As shown in Figure S11(b)–S11(d), there is no signature of exchange bias at 10, 130, and 180 K, analogous to that occurred in Cr-(Bi,Sb)₂Te₃/CrSb superlattices,[49] where the antiferromagnetic CrSb is magnetically ordered with spin texture altering from the bulk due to the interlay exchange coupling but without the interface exchange bias. Comparing these two systems, namely Fe₃GeTe₂/MnTe and Cr-(Bi,Sb)₂Te₃/CrSb, it is possible that the absence of the exchange bias in Fe₃GeTe₂/MnTe is associated with the magnetic order of MnTe (similar to CrSb), instead of antiferromagnetic state. However, such a detailed study requires neutron spectroscopy

and polarized neutron reflectometry measurements that are beyond the current scope of the work.

In summary, with MBE we successfully grew wafer-scale 8 nm 2D ferromagnetic Fe₃GeTe₂ films. Anomalous Hall effect and butterfly-like magnetoresistance verify that the easy axis is out-of-plane. The Curie temperature of the thin film is 216.4 ± 0.4 K. Through Fe doping, the Curie temperature can be adjusted. Further combined with antiferromagnetic MnTe, the coercive field increases 50% at 10 K. With distinct magnetic properties, wafer-scale and tunable high-Curie temperature 2D FMs are promising for spintronic devices and for the study of the proximity effect when coupling with other 2D materials.

## METHODS

### Thin film synthesis

Fe₃GeTe₂ thin films were grown on (0001) sapphire and (111) GaAs in a Perkin Elmer 430 MBE system with the base vacuum of 2.5 × 10⁻⁹ Torr. The substrates were cleaned using a general process before loaded into the chamber. The substrates were annealed at 600 °C for 30 min, and then decreased to the growth temperature of 340 °C. High-purity Fe (99.99%), Ge (99.999%), and Te (99.999%) at the temperature of 1165 °C, 1020 °C, and 285 °C, respectively, were co-evaporated from standard Knudsen cells. MnTe films were grown at the temperature of 320 °C with the Mn (99.99%) and Te (99.999%) cell temperature of 710 and 280 °C, respectively. The flux of each material is calibrated by the crystal oscillator. The MBE system is equipped with an in situ RHEED system.

### Thin film characterizations

Structural characterizations of Fe₃GeTe₂ and MnTe thin films were carried out by X-ray diffraction (Bruker D8 Discover, Bruker Inc., Billerica, MA, USA) and TEM (FEI Tecnai F20) equipped with EDS. Sample composition and

npj

Wafer-scale two-dimensional ferromagnetic Fe₃GeTe₂
Shanshan Liu et al.

6

concentration were determined by EDS. Cross-section TEM sample was prepared by FIB (FEI Scios DualBeam).

### Electrical and magnetization characterizations

The magneto-transport measurements were performed in physical properties measurement system (PPMS) by Quantum Design with a 9 T magnetic field. The devices were confined to the six-Hall-bar geometry. The data were collected using lock-in amplifiers (Stanford Research 830, Stanford Research Systems, Sunnyvale, CA, USA) in low frequency (<20 Hz). The magnetization measurements were accomplished in DC-superconducting quantum interface devices (SQUID) by quantum design with magnetic field up to 9 T.

### Data availability

The authors declare that all the relevant data are available within the paper and its Supplementary Information file or from the corresponding author upon reasonable request.

### AUTHOR CONTRIBUTIONS

F.X. conceived the ideas and supervised the overall research. S.L. and X.Y. synthetized high-quality Fe₃GeTe₂ thin films. S.L. and W.W. fabricated the devices. S.L., C.H., E.Z., J. L., Y.L., and C.Z. carried out the PPMS measurement. S.L., Y.S., and K.W. analyzed the transport data. Y.Z. and J.Z. did the TEM characterization. S.L. and F.X. wrote the paper with assistance from all other authors.

### ADDITIONAL INFORMATION

**Supplementary Information** accompanies the paper on the *npj 2D Materials and Applications* website (doi:10.1038/s41699-017-0033-3).

**Competing interests:** The authors declare no competing financial interests.

**Publisher's note:** Springer Nature remains neutral with regard to jurisdictional claims in published maps and institutional affiliations.

**Change history:** A correction to this article has been published and is linked from the HTML version of this article.

### REFERENCES

1. Zhang, Y., Tan, Y.-W., Stormer, H. L. & Kim, P. Experimental observation of the quantum Hall effect and Berry's phase in graphene. *Nature* **438**, 201–204 (2005).
2. Li, L. et al. Black phosphorus field-effect transistors. *Nat. Nanotechnol.* **9**, 372–377 (2014).
3. Radisavljevic, B., Radenovic, A., Brivio, J., Giacometti, V. & Kis, A. Single-layer MoS2 transistors. *Nat. Nanotechnol.* **6**, 147–150 (2011).
4. Jones, A. M. et al. Optical generation of excitonic valley coherence in monolayer WSe2. *Nat. Nanotechnol.* **8**, 634–638 (2013).
5. Ross, J. S. et al. Electrically tunable excitonic light-emitting diodes based on monolayer WSe2 p-n junctions. *Nat. Nanotechnol.* **9**, 268–272 (2014).
6. Wang, Z., Shan, J. & Mak, K. F. Valley- and spin-polarized Landau levels in monolayer WSe2. *Nat. Nanotechnol.* **12**, 144–149 (2016).
7. Efetov, D. K. et al. Specular interband Andreev reflections at van der Waals interfaces between graphene and NbSe2. *Nat. Phys.* **12**, 328–332 (2016).
8. Yokoya, T. et al. Fermi surface sheet-dependent superconductivity in 2H-NbSe2. *Science* **294**, 2518–2520 (2001).
9. Hsu, F.-C. et al. Superconductivity in the PbO-type structure α-FeSe. *Proc. Natl Acad. Sci.* **105**, 14262–14264 (2008).
10. Peng, R. et al. Tuning the band structure and superconductivity in single-layer FeSe by interface engineering. *Nat. Commun.* **5**, 5044 (2014).
11. Qing-Yan, W. et al. Interface-Induced high-temperature superconductivity in single unit-cell FeSe films on SrTiO3. *Chin. Phys. Lett.* **29**, 037402 (2012).
12. Park, J.-G. Viewpoint: opportunities and challenges of two-dimensional magnetic van der Waals materials: magnetic graphene? *J. Phys. Condens. Matter* **28**, 301001 (2016).
13. Jongh, L. J. de. Magnetic properties of layered transition metal compounds. in *Magnetic Properties of Layered Transition Metal Compounds* (ed. Jongh, L. J. de) 1–51 (Springer Netherlands, 1990).
14. Wolf, S. A. et al. Spintronics: a spin-based electronics vision for the future. *Science* **294**, 1488–1495 (2001).
15. Žutić, I., Fabian, J. & Das Sarma, S. Spintronics: fundamentals and applications. *Rev. Mod. Phys.* **76**, 323–410 (2004).
16. Barnaś, J., Fuss, A., Camley, R. E., Grünberg, P. & Zinn, W. Novel magnetoresistance effect in layered magnetic structures: theory and experiment. *Phys. Rev. B* **42**, 8110–8120 (1990).
17. Zhang, X. et al. Magnetic anisotropy of the single-crystalline ferromagnetic insulator Cr2Ge2Te6. *Jpn. J. Appl. Phys.* **55**, 033001 (2016).
18. Niu, J. et al. Anomalous Hall effect and magnetic orderings in nano-thick V5S8. *ArXiv161100584 Cond-Mat* (2016).
19. Zhu, X. et al. Signature of coexistence of superconductivity and ferromagnetism in two-dimensional NbSe2 triggered by surface molecular adsorption. *Nat. Commun.* **7**, 11210 (2016).
20. Zhuang, H. L., Kent, P. R. C. & Hennig, R. G. Strong anisotropy and magnetostriction in the two-dimensional Stoner ferromagnet Fe3GeTe2. *Phys. Rev. B* **93**, 134407 (2016).
21. Zhu, J.-X. et al. Electronic correlation and magnetism in the ferromagnetic metal Fe3GeTe2. *Phys. Rev. B* **93**, 144404 (2016).
22. Zhuang, H. L., Xie, Y., Kent, P. R. C. & Ganesh, P. Computational discovery of ferromagnetic semiconducting single-layer CrSnTe3. *Phys. Rev. B* **92**, 035407 (2015).
23. Siberchicot, B., Jobic, S., Carteaux, V., Gressier, P. & Ouvrard, G. Band structure calculations of ferromagnetic chromium tellurides CrSiTe3 and CrGeTe3. *J. Phys. Chem.* **100**, 5863–5867 (1996).
24. Li, X. & Yang, J. CrXTe 3 (X = Si, Ge) nanosheets: two dimensional intrinsic ferromagnetic semiconductors. *J. Mater. Chem. C* **2**, 7071–7076 (2014).
25. Chen, B. et al. Magnetic properties of layered itinerant electron ferromagnet Fe3GeTe2. *J. Phys. Soc. Jpn.* **82**, 124711 (2013).
26. May, A. F., Calder, S., Cantoni, C., Cao, H. & McGuire, M. A. Magnetic structure and phase stability of the van der Waals bonded ferromagnet Fe3-xGeTe2. *Phys. Rev. B* **93**, 014411 (2016).
27. Gong, C. et al. Discovery of intrinsic ferromagnetism in 2D van der Waals crystals. *ArXiv170305753 Cond-Mat* (2017).
28. Huang, B. et al. Layer-dependent ferromagnetism in a van der Waals crystal down to the monolayer limit. *ArXiv170305892 Cond-Mat* (2017).
29. Yang, S. et al. C3N—A 2D crystalline, hole-free, tunable-narrow-bandgap semiconductor with ferromagnetic properties. *Adv. Mater.* n/a-n/a (2017). doi:10.1002/adma.201605625.
30. Song, X., Hu, J. & Zeng, H. Two-dimensional semiconductors: recent progress and future perspectives. *J. Mater. Chem. C.* **1**, 2952–2969 (2013).
31. Yu, R. et al. Quantized anomalous hall effect in magnetic topological insulators. *Science* **329**, 61–64 (2010).
32. Liu, M. et al. Crossover between weak antilocalization and weak localization in a magnetically doped topological insulator. *Phys. Rev. Lett.* **108**, 036805 (2012).
33. Li, H. et al. The origin of bias independent conductance plateaus and zero bias conductance peaks in Bi2Se3/NbSe2 hybrid structures. *ArXiv160707731 Cond-Mat* (2016).
34. Hauser, J. J., Theuerer, H. C. & Werthamer, N. R. Proximity effects between superconducting and magnetic films. *Phys. Rev.* **142**, 118–126 (1966).
35. Zhu, Y., Pal, A., Blamire, M. G. & Barber, Z. H. Superconducting exchange coupling between ferromagnets. *Nat. Mater.* **16**, 195–199 (2016).
36. León-Brito, N., Bauer, E. D., Ronning, F., Thompson, J. D. & Movshovich, R. Magnetic microstructure and magnetic properties of uniaxial itinerant ferromagnet Fe3GeTe2. *J. Appl. Phys.* **120**, 083903 (2016).
37. Sbiaa, R., Law, R., Tan, Ei-Leen. & Liew, T. Spin transfer switching enhancement in perpendicular anisotropy magnetic tunnel junctions with a canted in-plane spin polarizer. *J. Appl. Phys.* **105**, 013910 (2009).
38. Sbiaa, R., Meng, H. & Piramanayagam, S. N. Materials with perpendicular magnetic anisotropy for magnetic random access memory. *Phys. Status Solidi RRL* **5**, 413–419 (2011).
39. Ziqan, A. M., Qasrawi, A. F., Mohammad, A. H. & Gasanly, N. M. Thermally assisted variable range hopping in Tl4S3Se crystal. *Bull. Mater. Sci.* **38**, 593–598 (2015).
40. Roy, A. et al. Structural and electrical properties of MoTe2 and MoSe2 grown by molecular beam epitaxy. *ACS Appl. Mater. Interfaces* **8**, 7396–7402 (2016).
41. Bao, L. et al. Quantum corrections crossover and ferromagnetism in magnetic topological insulators. *Sci. Rep.* **3**, 2391 (2013).
42. Nagaosa, N., Sinova, J., Onoda, S., MacDonald, A. H. & Ong, N. P. Anomalous hall effect. *Rev. Mod. Phys.* **82**, 1539–1592 (2010).
43. Stolichnov, I. et al. Non-volatile ferroelectric control of ferromagnetism in (Ga,Mn) As. *Nat. Mater.* **7**, 464–467 (2008).

Wafer-scale two-dimensional ferromagnetic Fe$_3$GeTe$_2$
Shanshan Liu et al.

7

44. Xiu, F. et al. Electric-field-controlled ferromagnetism in high-Curie-temperature Mn0.05Ge0.95 quantum dots. *Nat. Mater.* **9**, 337–344 (2010).
45. Chesnel, K., Wilcken, B., Rytting, M., Kevan, S. D. & Fullerton, E. E. Field mapping and temperature dependence of magnetic domain memory induced by exchange couplings. *New J. Phys.* **15**, 023016 (2013).
46. Kriegner, D. et al. Multiple-stable anisotropic magnetoresistance memory in antiferromagnetic MnTe. *Nat. Commun.* **7**, 11623 (2016).
47. Nogués, J. & Schuller, I. K. Exchange bias. *J. Magn. Magn. Mater.* **192**, 203–232 (1999).
48. Brown, H., Dahlberg, E. D. & Hou, C. Exchange bias measurements of CoFe/IrMn. *J. Appl. Phys.* **89**, 7543–7545 (2001).
49. He, Q. L. et al. Tailoring exchange couplings in magnetic topological insulator/antiferromagnet heterostructures. *Nat. Mater.* **16**, 94–100 (2016).